Earthquake-induced snow avalanches: II. Experimental study

Evgeny A. PODOLSKIY,[1] Kouichi NISHIMURA,[1] Osamu ABE,[2] Pavel A. CHERNOUS[3]

[1]*Graduate School of Environmental Studies, Nagoya University F3-1(200), Furo-cho, Chikusa-ku, Nagoya 464-8601, Japan*
E-mail: evgeniy.podolskiy@gmail.com
[2]*Snow and Ice Research Centre, National Research Institute for Earth Science and Disaster Prevention (NIED), 1400 Tokamachi, Shinjo 996-0091, Japan*
[3]*Center of Avalanche Safety, 'Apatit' JSC, 33a 50th Anniversary of October Street, 184250 Kirovsk, Russia*

ABSTRACT. We conducted experiments on the stability of snow, subjecting snow to vibrations, with the aim of improving our understanding of poorly studied mechanisms behind the triggering of avalanches during earthquakes. Most experiments were carried out on a specially constructed shaking table using artificial snowpacks containing a weak layer. Accelerations in the snow samples were measured using high-frequency sensors, enabling calculation of vibration-induced stresses within the snow at the moment of fracture. We used a high-speed camera to film different types of fracturing. In all cases, the vibrations caused failure of the snow by fracturing along the weak layer or at the base of the snow sample. An additional inertial stress induced by accelerations normal to the shear plane was quantified. We find that this stress can be related to smaller values of the shear strength in snow.

1. INTRODUCTION

Strong ground motion can trigger snow avalanches. A large area around an earthquake epicenter may be subject to sufficient shaking (associated with S-waves) to produce failure of the snow cover. In the case of artificial seismicity induced by technogenic explosions, the effective range of such shaking is several kilometers (personal communication from N.V. Barashev, 2009), but it is up to a few hundred kilometers for strong earthquakes (e.g. LaChapelle, 1968; Higashiura and others, 1979; Singh and Ganju, 2002; Podolskiy and others, 2010). Avalanches due to either of these types of seismicity may claim human lives (Singh and Ganju, 2002; personal communication from N.V. Barashev, 2009), block roads (LaChapelle, 1968; Higashiura and others, 1979; Ogura and others, 2001) or perturb the mass balance of glaciers (Tarr and Martin, 1914). Podolskiy and others (2010) describe snow avalanches triggered by natural or artificial seismicity; importantly, they also note the lack of any comprehensive understanding of the mechanisms involved in triggering these events.

Previous attempts to understand the effects of seismicity on snowpack stability have included avalanche studies in the Khibiny mountains, Russia (Chernous and others, 1999, 2002, 2004, 2006; Mokrov, 2008), experimental work in Japan (Abe and Nakamura, 2005; Nakamura and others, 2010) and theoretical work on the reduction in the stability index during shaking (Ogura and others, 2001; Matsuzawa and others, 2007). The importance of a high rate of shear loading has been demonstrated by Abe and Nakamura (2005), and further work is in progress (to be published elsewhere). However, the available information on the effects of seismicity on stressed snow is limited by a lack of detailed and precise measurements. Fundamental questions remain regarding the processes that underlie the fracturing of snow during shaking. Indeed, aside from two events described by Higashiura and others (1979) and Ogura and others (2001), earthquake-induced avalanches have not been documented in association with well-documented seismic records, details of the snow stratigraphy or the response of steep mountain slopes to strong ground motion (Podolskiy and others, 2010). Therefore, many of the theoretical assumptions in this field of study remain speculative, and more detailed experimental work must be undertaken to understand the nature of the response of snowpacks to strong ground motion.

We performed laboratory studies to quantify how vibrations (simulating strong ground motion) influence snow stability. The experiments were conducted in the Cryospheric Environmental Simulator (CES) at the Shinjo Branch of the Snow and Ice Research Centre at the National Research Institute for Earth Science and Disaster Prevention (NIED), Japan. We describe and discuss the shaking-table experiments, the methods and equipment used and the results obtained.

2. METHODS

The method involved in our experiments requires the preparation of snow samples with potential weak layers and subjecting these to vibrations on a shaking table (Figs 1–3). The tests call for a variety of shaking modes. First, we considered the simplest case of shaking, which allowed only a single degree of freedom and oscillations in the horizontal direction. The shaking table was set at different inclinations. Second, we considered the more complex case of a double degree of freedom, with both horizontal and vertical components of acceleration, but with the shaking table always in the horizontal position. Our experiments with artificial snow were undertaken at a constant air temperature of –10°C and a constant relative humidity of 73%.

2.1. Artificial 'sandwiches' of snow with a weak layer

Weak layers within a snowpack provide localized planes of shear that facilitate slab avalanche formation. For this reason we included a weak layer in our artificial snow samples for experiments on the shaking table. The snow we used was specially prepared at the CES snowfall facility. First, we grew artificial stellar dendrites (PPsd; the code numbers used here are taken from the classification proposed by Fierz and others, 2009); on settling, these evolved into partly decomposed particles (DFdc), or, if the settling took place under a load, highly broken particles (DFbk). The weak layer was

https://doi.org/10.3189/002214310792447833 Published online by Cambridge University Press

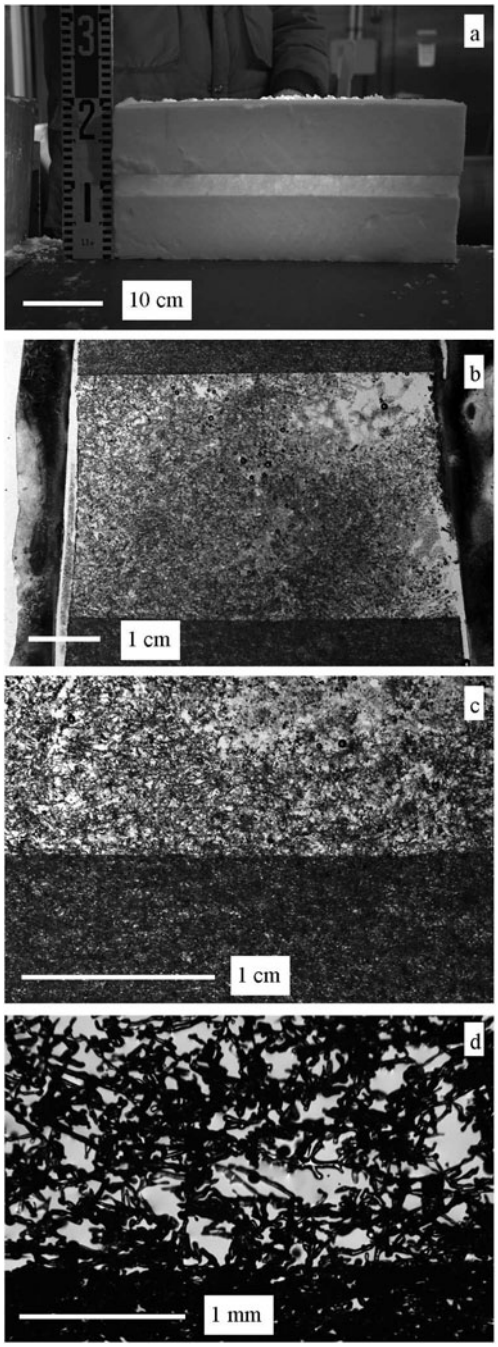

Fig. 1. Photographs of an artificial weak layer between two blocks of denser snow (block I): (a) vertical cross-section through the artificial 'sandwich' with a lamp behind it to show the weak layer; (b) aniline ($C_6H_5NH_2$) 1 mm thick vertical cross-section of the weak layer; (c, d) microphotographs of the contact area between the bottom part of the weak layer (DFdc) and more dense snow (DFbk), which acted as the shear plane for most of the observed fracturing.

prepared by sifting a 5 cm layer of fresh snow (DFdc) through a close-meshed sieve over a block of compacted homogeneous snow (DFbk; 0.87 m × 0.87 m), putting another block of compacted homogeneous snow (DFbk) on top of the fresh snow, and leaving the samples to sinter for either 50 or 74 hours. This simple procedure allowed the weak layer of the 'sandwich' to settle and therefore strengthen the connection to the adjacent blocks (Fig. 1). Altogether, five large 'sandwiches' were prepared for vibration testing, with average densities of 222 kg m^{-3} in the lower blocks, 100 kg m^{-3} in the weak layers and 210 kg m^{-3} in the upper

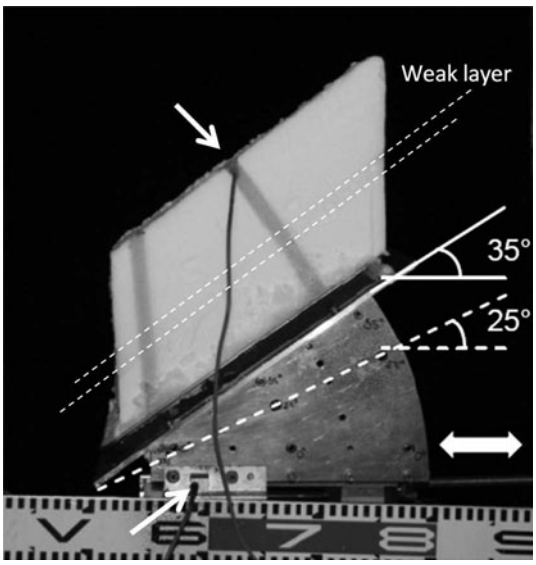

Fig. 2. The shaking table adjusted for horizontal oscillations and different inclinations (0°, 25° or 35°) and with a 'sandwich' type of snow block frozen to the metal platform and cut according to the inclination (35° in this photo). Small arrows indicate two accelerometers (installed horizontally). All blocks were dyed (vertical and normal bands) to aid in visualization of fracturing. Double-headed arrow indicates the direction of shaking.

blocks (Table 1). The 'sandwiches' were then cut with a snow saw to form smaller blocks (length 0.29 m, width 0.20 m, height 0.17 m) which were frozen onto metal plates that had been warmed outside the cold laboratory to ~23°C. This process firmly fixed the blocks to the shaking platform, ready for vibration testing. Samples used in tests on an inclined shaking platform (to simulate the natural shearing produced in snow subject to the force of gravity on a slope) were cut before mounting according to the selected slope angle (25° or 35°). All the blocks were characterized by two potential planes of shearing (the weak layer and the bottom surface of the block). This is reflected in the test results, where similar shear strengths of both these planes were observed (shown later). We could have concentrated fracturing in the weak layers by making the lower part of the 'sandwich' much denser and harder.

2.2. Shaking table and main adjustment modes

One of the basic tasks of earthquake engineering is to calculate the loading produced by the acceleration applied to the mass of a building during an earthquake; in other words, to calculate the inertial force. The inertial force must be known, for example, if one is to design a structure capable of standing up in an earthquake (Reitherman, 1997). We used the shaking table to observe the destabilization of snow, thereby enabling us to calculate the inertial forces involved.

The shaking table was specially constructed with horizontal and vertical oscillations driven by an electric motor (an increase in frequency increased the peak acceleration). The platform of the table could be adjusted for different modes of shaking (i.e. shaking with one degree of freedom, involving horizontal oscillations only, or shaking with two degrees of freedom, involving horizontal and vertical oscillations). The amplitude of shaking was 33 mm horizontally and 14 mm vertically. Different inclinations of shaking platform (0°, 25° and 35°) were considered for single degree-of-freedom mode (Fig. 2). The direction of

https://doi.org/10.3189/002214310792447833 Published online by Cambridge University Press

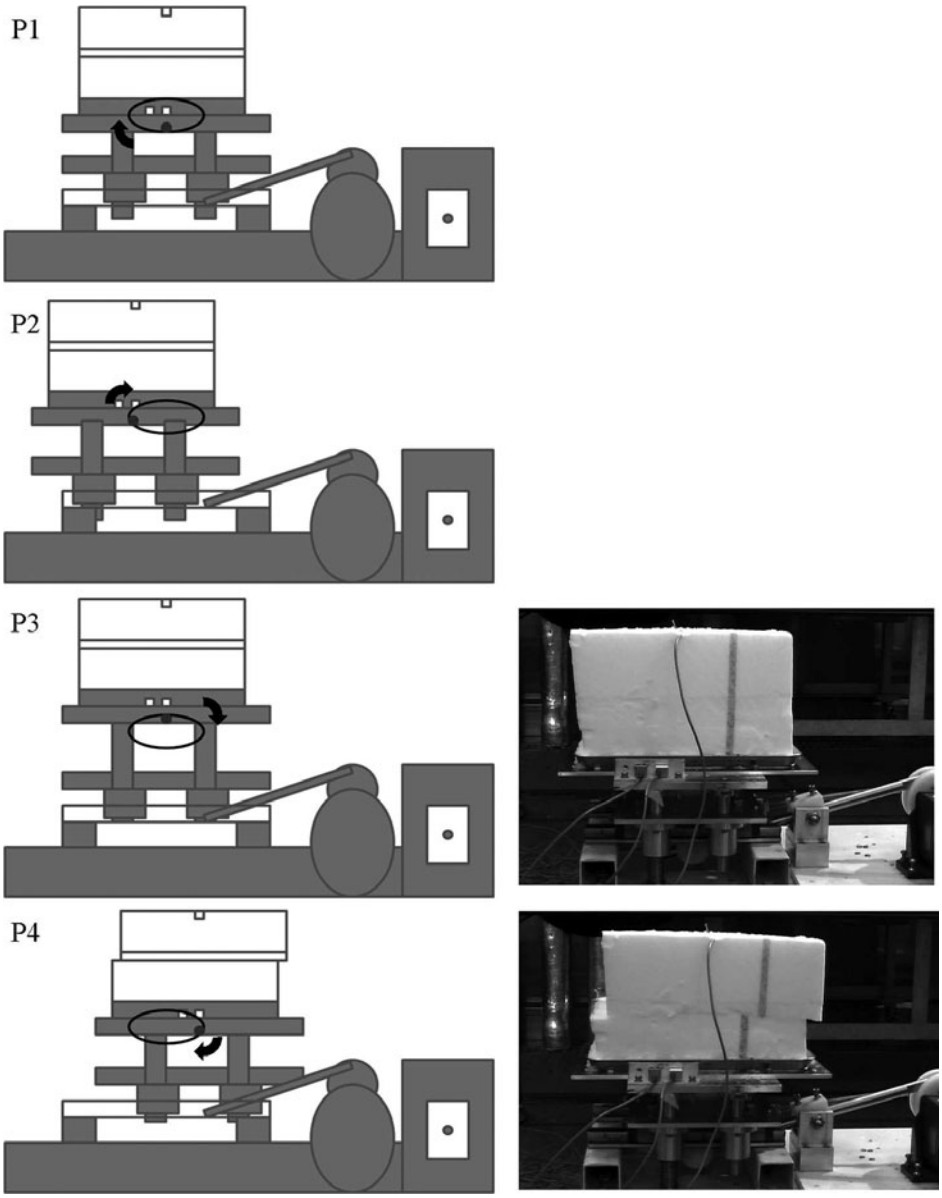

Fig. 3. Pattern of the shaking-table clockwise oscillations for one full cycle before fracture (P4) and the principal points of trajectory P1–P4 (reference point is shown by dot on the ellipse, which represents the trajectory of the shaking platform, and arrows indicate the direction of movement). Frames of a video record show a snow sample before (P3) and after (P4) fracture.

Table 1. Characteristics of artificial snow samples (all of which were 'sandwiches' with a weak layer) used for the shaking-table tests. All snow samples were prepared following exactly the same method, yet some unavoidable variations in parameters exist. For example, variations in the density of the weak layers may have arisen because it is difficult to measure density due to the small thickness of the horizon. For this reason, we provide mean values for an average sample

Block number	Date of test	Average density of bottom block	Average density of weak layer	Average density of top block	Morphological classification bottom/weak layer/top	Average size of shaken samples			
						Length	Width	Height	Shear plane area
		$kg\,m^{-3}$	$kg\,m^{-3}$	$kg\,m^{-3}$		cm	cm	cm	m^2
I	11 Dec 2008	229	90	223	DFbk/DFdc/DFbk	29.4	0.2	17.7	0.0594
II	12 Dec 2008	180	90	174	DFbk/DFdc/DFbk	29.6	19.8	20.4	0.0597
III	15 Jul 2009	228	85	226	DFbk/DFdc/DFbk	30.2	19.7	15.2	0.0597
IV	16 Jul 2009	244	117	218	DFbk/DFdc/DFbk	29.6	20.1	14.7	0.0597
V	17 Jul 2009	231	120	212	DFbk/DFdc/DFbk	30.0	19.8	15.9	0.0593
Average sample		222	100	210	DFbk/DFdc/DFbk	29.8	19.9	16.78	0.0596

https://doi.org/10.3189/002214310792447833 Published online by Cambridge University Press

Table 2. Summary of observed types of fractures and total number of similar fractures. These are classified according to the type of oscillation, inclination, location of fracturing (within the bottom or weak layers) and the 'background' normal stress at the moment of fracture. A dash indicates a type of fracturing that is impossible for the particular mode of oscillation. d.f., degree of freedom

Type of oscillation	Inclination of shaking platform	Single fractures				Double fractures				Total number B/WL
		Bottom (B)		Weak layer (WL)		Bottom (B)		Weak layer (WL)		
		Positive normal pressure	Negative normal pressure	Positive normal pressure	Negative normal pressure	Positive normal pressure	Negative normal pressure	Positive normal pressure	Negative normal pressure	
Single d.f.	0°	2	–	11	–	2	–	2	–	4/13
25°	0	1	0	0	0	3	2	1	4/3	
35°	0	2	0	3	0	0	0	0	2/3	
Double d.f.	0°	0	7	0	7	0	0	0	0	7/7
										17/26

shaking was always applied parallel to the longest side of the platform. During shaking with two degrees of freedom, the platform was always left in the horizontal position (Fig. 3). The oscillation frequency could be increased slowly or quickly to measure the effects of the rate of increase on peak accelerations (see section 3.2.5).

2.3. Principal measurements (accelerations and snow parameters)

Two horizontal components of acceleration (at the base and top of snow samples) and one vertical component (at the base, only in the case of tests with two degrees of freedom) were recorded continuously using 'Kyowa' AS-10/20HB acceleration transducers Fig. 3) at a sampling interval of 1 or 2 ms. When the shaking table was inclined at 25° or 35°, the acceleration transducer was always installed horizontally in the snow (following established practice in shaking-table tests related to landslide studies (e.g. Asano and others, 2003)). Before we analyzed the results, the acceleration records were calibrated and the fast Fourier transform (FFT) power spectra calculated (a rectangular time window was used). The acceleration records (denoted x_s, base x_b, base z_b) display asymmetric amplitudes because of the inherent mechanical properties of the shaking table, but also in part because of the increased viscosity of the oil due to the low temperature of –10°C.

A high-speed camera ('NAC C3' HSV 500, synchronized with a stroboscope) was used to determine the movement pattern of the shaking table and the precise moment of snow fracturing. The recording frequency was 250 Hz.

For every test, we measured the mass, density, size of the snow block and area of shear plane failure, in order to calculate the shear strength of the snow and to determine the principal stresses at the moment of fracture. Toxic aniline was used to make 2-D cross-sections of the weak layer (Fig. 1b–d) in order to characterize and visualize the microstructure of the snow (Kinosita and Wakahama, 1960).

3. RESULTS AND DISCUSSION

3.1. Video record of fractures

We could detect the occurrence of fractures with the aid of video records (e.g. Figs 3 and 4) by comparing these with the records of acceleration and by noting the abrupt disagreement between acceleration signals in the snow and on the shaking platform. With the help of this information, we were able to determine the peak accelerations responsible for fracturing, as discussed in more detail below.

The two principal types of fracturing (Table 2) are single fractures, which develop either along the bottom of the snow block (also reported by Abe and Nakamura, 2005; Nakamura and others, 2010) or along the weak layer; and double fractures, which develop in two stages, first along the shear plane at the bottom of the lower specimen (primary fracturing) and then during the next phase of shaking, along the weak layer (secondary fracturing). For the complete set of our experiments, 40% of fractures occurred along the bottom and 60% along the weak layer; only a few double fractures were observed. Fracturing at the base of natural packs of snow and within natural weak layers is known to occur during real earthquake-induced avalanching. For example, avalanche failure along the base was documented by Ogura and others (2001), failure along weak layers was described by Higashiura and others (1979) and both types were described by LaChapelle (1968).

We define tension as negative normal pressure, and compression as positive. In the present tests with an inclined shaking table, all primary and most secondary fracturing occurred under negative normal pressures (see section 3.2.1) and only two secondary fractures (along weak layers) developed during compression. As a consequence of primary fracturing, the platform and the block of fractured snow started moving relative to each other. This corresponded to a reduction in friction during the initial stage of downslope movement of the block of fractured snow. Double fractures developed before snow started to move.

Video records of double degree-of-freedom oscillations demonstrate that the vibrations of the shaking table display a clockwise elliptical trajectory. The snow block acts as a rudimentary and rather stiff oscillator; it simply moves with the shaking table. The single particle trajectory of the shaking platform and its speed as tracked by video analysis correspond well with measured accelerations, showing the same asymmetry (see section 2.3) at higher frequency for the segment P3–P4–P1 and at lower speeds for P1–P2–P3 (Fig. 3). Owing to this movement, all fractures occur at the same trajectory point, P4, where the shear and tensile forces applied to the snow sample reach a maximum value (Fig. 3) (see sections 3.2.3 and 3.2.4).

https://doi.org/10.3189/002214310792447833 Published online by Cambridge University Press

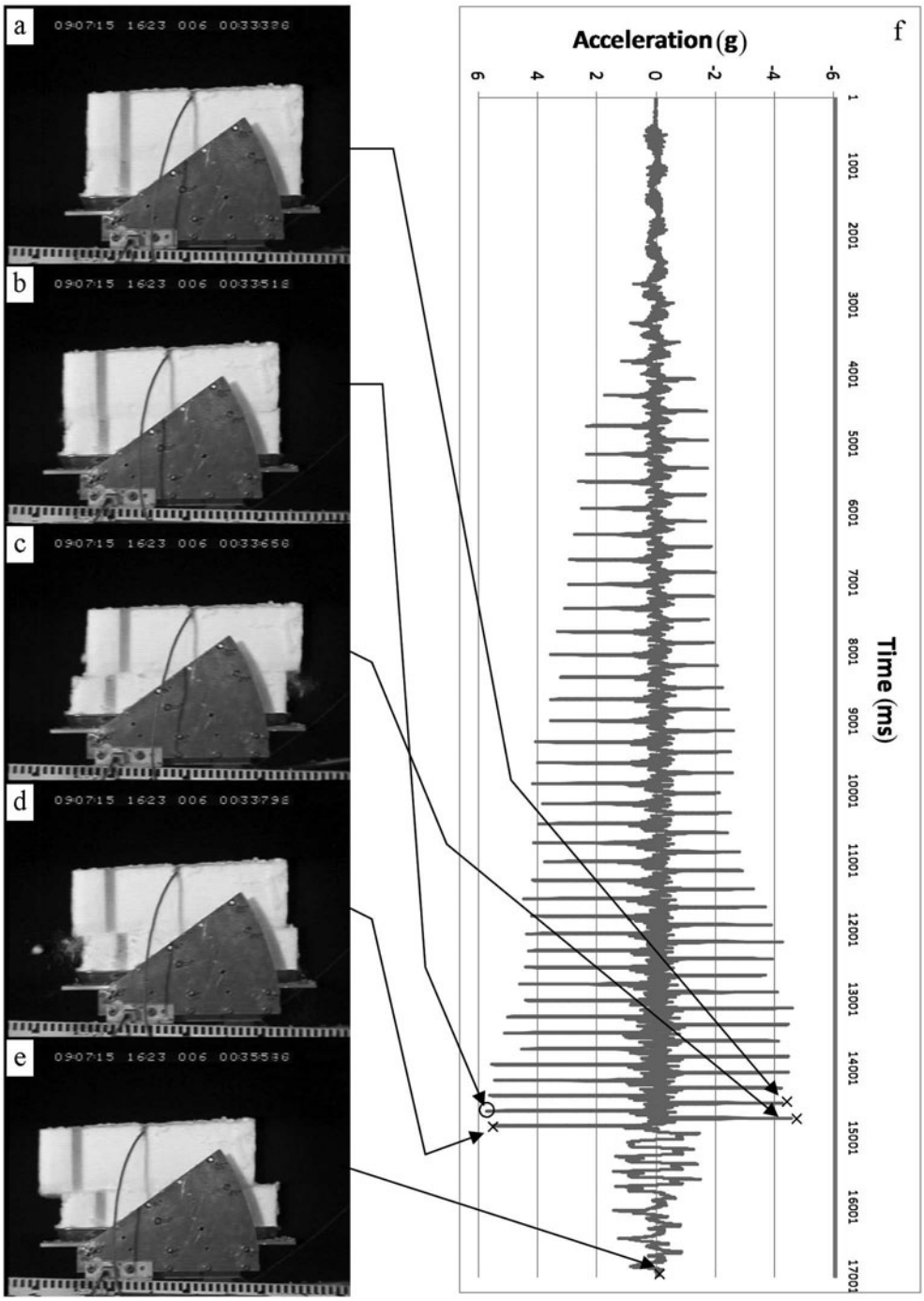

Fig. 4. Sequence of high-speed video frames (a–e) showing (b) the moment of snow sample fracture under single degree-of-freedom horizontal oscillations (sample 20; Table 3). Long arrows indicate the moments corresponding to the accelerogram (f). The circle in (f) indicates fracture nucleation (b).

3.2. Oscillations and fracturing of the snow sample

3.2.1. Shear stress caused by shaking

When the shaking table moves the base of a frozen snow sample, its mass experiences inertia, since the snow attempts to follow the motion of the shaking table. Therefore, the maximum of an applied force corresponds to the peak acceleration, a_p (as deduced from high-speed video records and accelerograms (e.g. Fig. 4)) at the instant when the shaking platform reverses direction. Horizontal accelerations of a shaking table give rise to shear stresses within the snow sample and since the acceleration reverses due to the trajectory of the shaking platform, the direction of shear stresses also reverses (always for horizontal tests and almost always for inclined tests). By dividing applied inertial force by the area of the plane of shearing (Abe and Nakamura, 2005; Nakamura and others, 2010) (Fig. 5), the critical shear strength of the snow can be calculated:

$$\tau = \frac{m_f a_p g}{A} \quad (1)$$

where τ is the shear strength, m_f is the mass of fractured snow, a_p is the peak acceleration causing fractures (e.g. Fig. 6), g is the gravitational acceleration and A is the area of the shear plane. These values were determined from our test records or measured directly during testing.

https://doi.org/10.3189/002214310792447833 Published online by Cambridge University Press

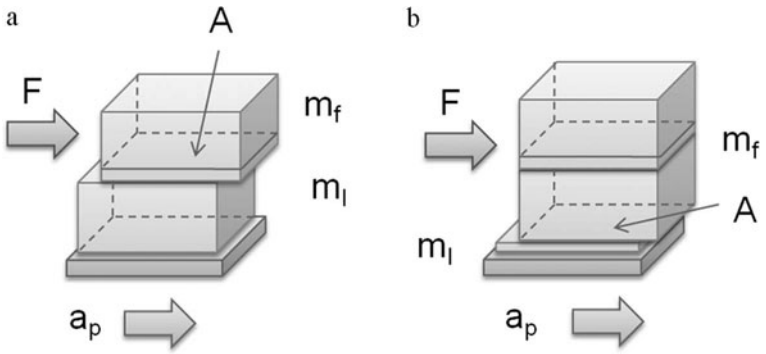

Fig. 5. Conceptual model for calculating the shear stress (and shear strength) during the application of inertia to a snow block causing fracturing (a) along the weak layer and (b) along the bottom. F is the force applied to snow by inertia, a_p is the horizontal peak acceleration, m_f is the mass of fractured snow, m_l is the mass of snow left after fracturing and A the area of the shear fracture surface.

For tests with an inclined shaking table, the natural shearing, τ_n, due to a mass of snow over the shear plane should be included (Fig. 7a) and it is given by

$$F = \tau_n A$$

$$\tau_n = \frac{m_f g \sin\alpha}{A}. \quad (2)$$

The resulting net force and its direction are determined by the sum of force vectors produced by acceleration τ_{ap} and the weight of snow in the gravitational field (Fig. 7b). This vector sum applied to a mass of snow can be broken down into two components, shearing, τ_{st}, and the normal to the shear plane, where

$$\tau_{st} = \frac{m_f g a_p \cos\alpha + m_f g \sin\alpha}{A}. \quad (3)$$

Most of the shear strength values (within 2σ) calculated in the present study fall in the range 1.0–2.4 kPa (Table 3). The values are high compared with values for dry coherent snow presented by Mellor (1975), demonstrating that microstructure is more important in influencing strength than is density (e.g. Voitkovskiy and others, 1975; Schweizer and others, 2003).

The orientation of the slope of the shaking table determined the principal direction of the net force, and most of the fractures occurred at the furthest left-hand point of the shaking-table trajectory (Fig. 2). At this point we always had stress conditions, which not only shear the snow but also pull the block away from the slope, i.e. a negative normal pressure or tension, σ_t (Fig. 7b), where σ_t is expressed as

$$F = \sigma_t A$$

$$\sigma_t = \frac{m_f g \cos\alpha - m_f g a_p \sin\alpha}{A}. \quad (4)$$

During the opposite phase of oscillation (at the furthest right-hand point of the shaking-table trajectory), the block of snow is pushed into the slope (i.e. an increase in normal pressure or compression, σ_c; Fig. 7c), where

$$\tau_{sc} = \frac{m_f g a_p \cos\alpha - m_f g \sin\alpha}{A} \quad (5)$$

and

$$\sigma_c = \frac{m_f g \cos\alpha + m_f a_p g \sin\alpha}{A}. \quad (6)$$

Only two secondary fractures, in samples 32 and 33 (Table 3), were observed from video records to form at this phase of oscillation. (If compared with the static condition, the normal pressure was three times higher at the moment of fracture, though it was smaller than the compressive strength of snow and was not a direct cause.)

3.2.2. Measured accelerations

An FFT power spectrum analysis of the obtained accelerograms shows a significant number of maxima falling within the frequency range 2–3 Hz. This can be related to the number of oscillations performed by the shaking table (Fig. 6). Even though the prevailing maximum values for the response spectra of the shaking table (e.g. 2.7 Hz) are higher than the absolute values of ground response typical for earthquakes (e.g. Kramer, 1996), the range of loading times (the time interval ~50 ms during which inertia was applied consequential to a reversal of the movement vector of the shaking table) still yields brittle fracture in snow (e.g. Föhn and Camponovo, 1997).

The measured peak horizontal accelerations responsible for fractures vary from 1.92 to 7.03 g (Fig. 8). The peak vertical accelerations at the moment of fracturing range from 0.41 to 2.37 g (Table 3). Given that the extremes for natural peak ground accelerations observed anywhere in the world are between 1.0 g and 3.0 g for horizontal accelerations (Anderson, 2003) and 3.8 g for vertical accelerations (Aoi and others, 2008), the accelerations in our experiments are rare or too high for natural seismicity. However, it was necessary to subject our small and low-mass snow samples to such high accelerations (Table 3) because the induced shear force is proportional to the mass of the snow sample (Equation (1)). This explains why heavier samples fracture at lower values of peak acceleration and why there is no relationship between shear strength and peak acceleration (Fig. 8). If larger masses of snow were used over the shear plane, much smaller values of acceleration, closer to natural tremors, would suffice for fracturing (see section 3.3).

3.2.3. Normal stress oscillations under double degree-of-freedom shaking

The stress state of the snow block under double degree-of-freedom oscillations can be discussed in terms of both normal and shear stresses and it is of interest to estimate the contributions of these stresses to the stress tensor. If we adopt the common geological convention of treating compressive stress as positive normal pressure and tensile stress as negative, it is possible to represent them both on one axis of

https://doi.org/10.3189/002214310792447833 Published online by Cambridge University Press

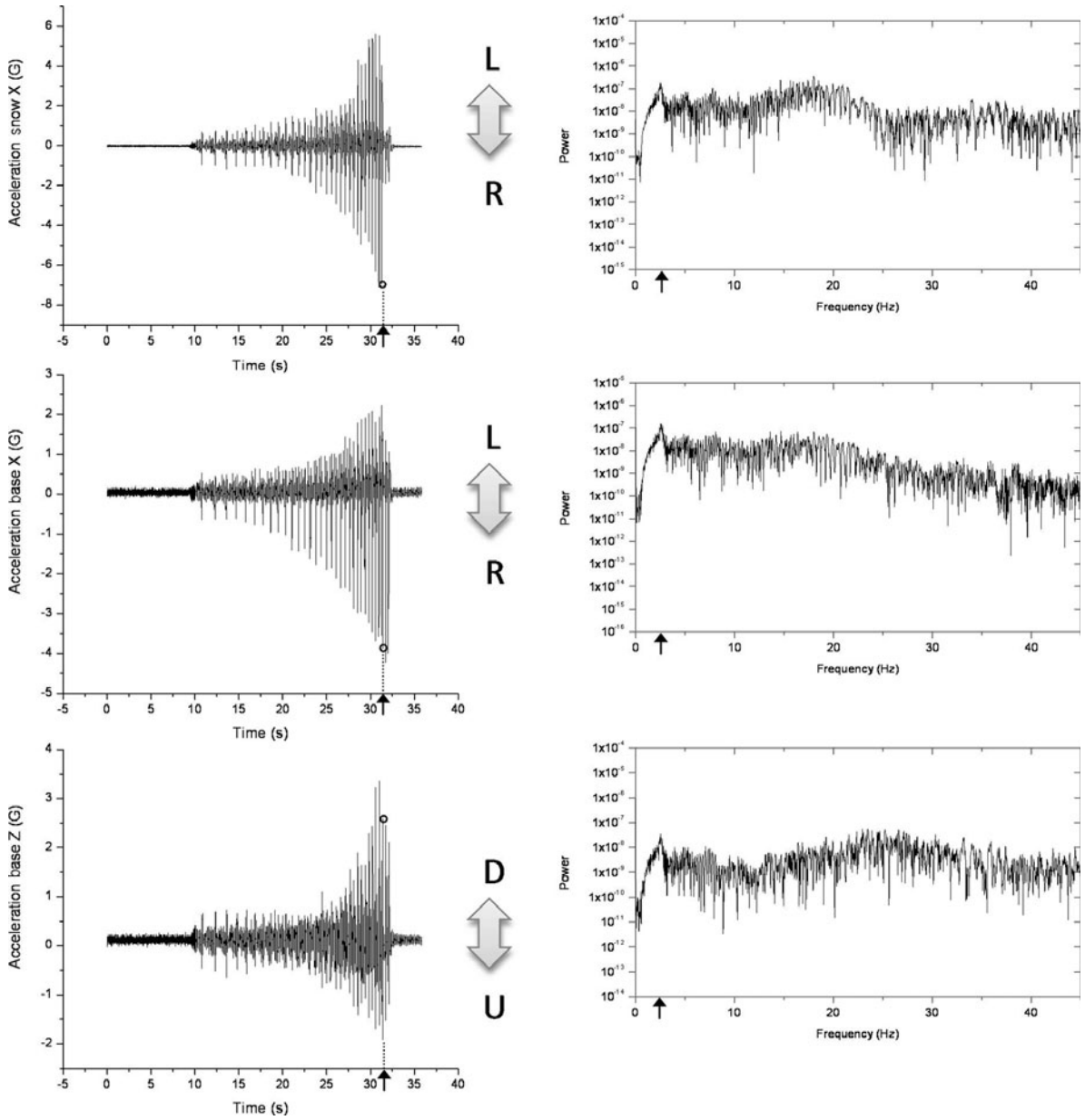

Fig. 6. Example of acceleration records and FFT power spectra for an experiment on the shaking table (sample 1). The instant of fracturing is shown by an arrow and a circle. Arrows indicate the dominant ranges of vibration frequency. Double-headed arrows indicate directions of measured accelerations.

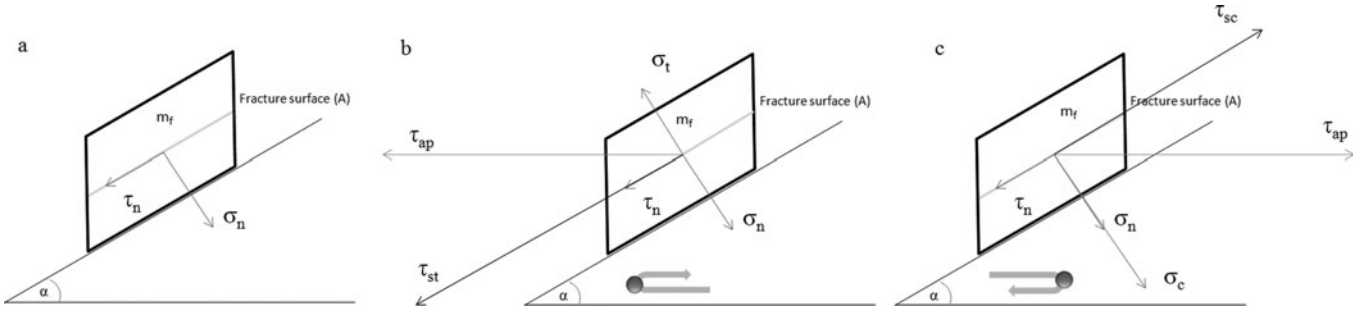

Fig. 7. (a) Stresses in a snowpack due to weight without shaking. (b, c) Principal stress tensor components at the moment of fracture: (b) fracturing typical in most of the tests at the left side of the trajectory with negative normal pressure and (c) possible fracturing at the right side with increased normal pressure. m_f is the mass of the fractured snow block, σ_n is the normal shearing caused by the mass of snow along the shear plane, τ_{ap} is the force produced by acceleration, τ_{st} and τ_{sc} are the shear components of the net force, σ_t is the tensile component of the net force, σ_c is the compressive component of the net force, A is the area of the shear plane, α is the slope inclination (angles and lengths of vectors are not absolute values; the dot on the curved arrow indicates the point of oscillation).

https://doi.org/10.3189/002214310792447833 Published online by Cambridge University Press

Table 3. Principal measured and calculated parameters for vibration-induced fractures

Sample number	Block number	Type of test*	Inclination	Type of fracture†	Mass of fractured snow, m_f	Shear plane area, A	Peak horizontal acceleration, a_p	Peak vertical acceleration	Total time of vibration until fracture	Shear strength, τ	Natural shear, τ_n	Normal pressure before fracture, σ_n	Normal pressure at the moment of fracture, $\sigma_{n,c,t}$	Critical thickness of snow, h_{cr}, for 0.5 g and 38°
			°		kg	m^2	g	g	s	Pa	Pa	Pa	Pa	m
1	I	D	0	WL	1.24	0.059	7.03	2.37	21.5	1441.4	0.0	206.1	–485.9	0.66
2	I	D	0	WL	1.24	0.060	6.74	1.83	21.5	1354.2	0.0	202.7	–367.7	0.62
3	I	D	0	WL	1.26	0.061	6.45	1.85	9.3	1303.2	0.0	202.6	–372.7	0.59
4	I	D	0	WL	1.22	0.061	6.68	1.80	5.5	1310.0	0.0	196.1	–352.9	0.60
5	I	D	0	WL	2.54	0.060	2.67	0.76	2.2	1100.1	0.0	415.1	–313.1	0.50
6	I	D	0	WL	2.70	0.058	2.24	0.41	2.2	1022.5	0.0	456.5	–187.2	0.47
7	I	D	0	WL	2.42	0.055	2.73	0.51	2.2	1160.5	0.0	431.5	–216.8	0.53
8	II	D	0	B	2.02	0.058	5.81	1.60	30.8	1984.3	0.0	341.5	–540.4	1.15
9	II	D	0	B	1.82	0.060	6.57	0.89	41.0	1931.7	0.0	297.5	–261.7	1.12
10	II	D	0	B	3.05	0.058	3.46	2.28	4.7	1773.2	0.0	515.7	–1168.5	1.03
11	II	D	0	B	2.62	0.059	4.32	2.53	12.6	1870.1	0.0	435.5	–1095.2	1.09
12	II	D	0	B	1.42	0.057	6.44	1.72	11.2	1552.3	0.0	244.3	–414.6	0.90
13	II	D	0	B	1.50	0.060	5.84	0.79	6.6	1420.5	0.0	245.2	–192.2	0.82
14	II	D	0	B	1.68	0.055	7.00	1.43	6.7	2065.0	0.0	299.5	–422.0	1.20
15	III	S	0	B	1.60	0.059	5.83	0.00	26.0	1543.9	0.0	264.8	264.8	0.69
16	III	S	35	B	2.86	0.062	2.96	0.00	9.3	1361.4	260.4	372.0	–399.0	0.61
17	III	S	0	WL	2.06	0.057	5.56	0.00	18.6	2026.6	0.0	356.2	356.2	0.91
18	III	S	25	B	3.11	0.062	3.33	0.00	6.7	1699.0	208.7	447.5	–247.4	0.76
19	III	S	35	WL	1.34	0.061	2.23	0.00	7.2	521.0	124.6	177.9	–99.9	0.23
20	III	S	0	WL	2.25	0.059	5.72	0.00	14.2	2130.2	0.0	372.4	372.4	0.95
21	III	S	35	B	2.90	0.061	3.04	0.00	9.2	1422.3	266.3	380.3	–429.2	0.64
22	III	S	25	B	2.78	0.058	3.38	0.00	10.0	1626.6	197.2	422.9	–243.6	0.73
23	III	S	0	WL	2.02	0.059	4.96	0.00	9.6	1658.3	0.0	334.3	334.3	0.74
24	III	S	25	WL	1.98	0.062	2.53	0.00	6.8	850.1	132.9	284.9	–51.2	0.38
25	IV	S	0	WL	2.18	0.058	6.36	0.00	9.8	2363.6	0.00	371.6	371.6	1.10
26	IV	S	35	WL	2.20	0.058	3.52	0.00	4.8	1292.2	214.3	306.2	–448.5	0.60
27	IV	S	35	WL	2.22	0.060	3.62	0.00	8.6	1283.9	208.1	297.2	–456.1	0.59
28	IV	S	25	B	2.82	0.060	5.06	0.00	8.7	2299.1	194.0	416.0	–565.6	1.07
29	IV	S	25	B	2.80	0.060	4.52	0.00	8.4	2255.2	194.2	416.6	–461.4	1.04
30	IV	S	0	WL	2.11	0.063	5.05	0.00	8.0	1652.9	0.00	327.3	327.3	0.77
31	IV	S	0	WL	2.12	0.060	5.33	0.00	5.7	1859.3	0.00	348.8	348.8	0.86
32	IV	S	25	WL	1.92	0.060	4.47	0.00	8.7	1134.1	132.0	283.3	873.6	0.53
33	IV	S	25	WL	2.04	0.060	4.26	0.00	8.4	1151.5	141.5	303.5	906.4	0.53
34	V	S	0	B	2.93	0.060	4.45	0.00	6.1	2124.0	0.0	477.3	477.3	1.01
35	V	S	0	WL	2.42	0.059	5.91	0.00	5.4	2397.5	0.0	405.7	405.7	1.14
36	V	S	0	B	2.79	0.058	4.75	0.00	4.2	2249.7	0.0	473.6	473.6	1.07
37	V	S	0	WL	3.50	0.061	3.51	0.00	4.7	1960.2	0.0	558.5	558.5	0.93
38	V	S	0	B	2.89	0.060	3.77	0.00	4.3	1773.5	0.0	470.4	470.4	0.84
39	V	S	0	WL	4.60	0.059	2.70	0.00	2.8	2051.2	0.0	759.7	759.7	0.98
40	V	S	0	WL	4.54	0.059	2.80	0.00	3.2	2130.9	0.0	761.1	761.1	1.02
41	V	S	0	WL	4.03	0.059	2.63	0.00	2.9	1767.7	0.0	672.1	672.1	0.84
42	V	S	0	WL	2.29	0.058	5.55	0.00	4.2	2157.5	0.0	388.7	388.7	1.03
43	V	S	0	WL	2.40	0.060	4.41	0.00	4.3	1722.9	0.0	390.7	390.7	0.82

*S, single degree-of-freedom oscillations; D, double degree-of-freedom oscillations.
†WL, weak layer; B, bottom.

normal stress (acting in the shear plane). Oscillation of normal stress is a function of the vertical component of acceleration. Considering only the normal stress variations between principal points of the shaking-table trajectory (P1–P4; Fig. 3), we can see two points with normal stress under normal gravity (P1 and P3, around 0.3 kPa), one point with compressive stress due to an upward movement and increasing weight (P2, around 0.7 kPa; insufficient to reach the compressive strength (Mellor, 1975)) and one point with tensile stress normal to the shear plane due to a downward movement with significant negative vertical acceleration (P4, around 0.45 kPa). If we show on one diagram (Fig. 9) the shear and normal stress oscillations for one full oscillation before fracture, we find that the fracturing of blocks of snow always occurs at the particular shear stress and shear strength reached at a point in the shaking-table trajectory (P4) that induced a negative normal stress (tensile stress) (Table 3).

https://doi.org/10.3189/002214310792447833 Published online by Cambridge University Press

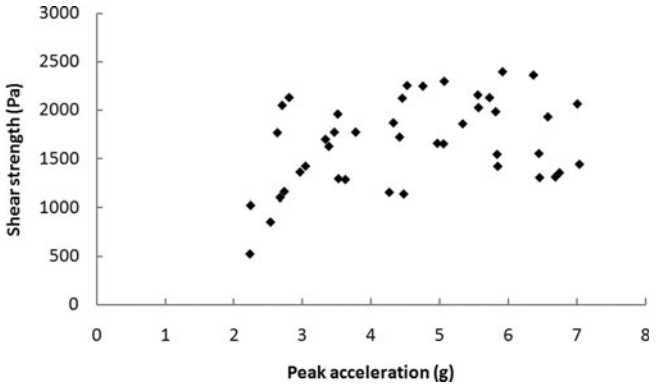

Fig. 8. Peak horizontal accelerations compared with the corresponding shear strengths.

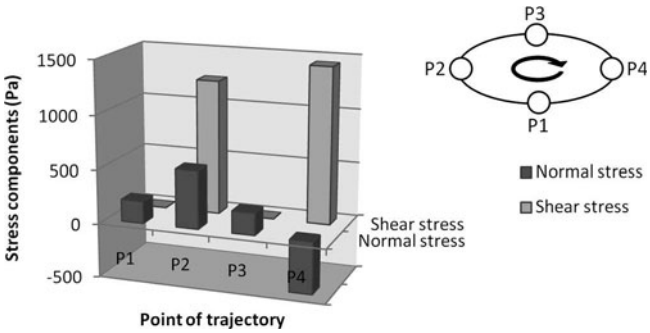

Fig. 9. Example of oscillations of shear and normal stress as a function of horizontal and vertical components of acceleration between the principal points on the trajectory (P1–P4) for one full cycle of the platform's oscillation before fracture (for a double degree-of-freedom test, sample 1). Principal points of the trajectory are shown on the ellipse. The arrow marks the direction of the platform's movement. P4 corresponds to the point of fracture (see Fig. 3 for more details).

3.2.4. Significance of normal stress oscillations

When adopting the same convention as described above to represent stresses for all tests, we can see differences between tests with and without normal stress oscillations (Fig. 10). If we compare the shear strength values with the normal stress for different tests and types of fracturing, we see that almost all fractures for inclined or double degree-of-freedom tests formed when the normal pressure was negative (Fig. 10b–d and f–h). The absolute values of these tensile stresses were smaller than the values of the shear strength of snow and, if we assume that the tensile strength of low-density snow is higher than the shear strength (Mellor, 1975), they would seem to be insufficient to reach the tensile strength of the snow samples. Mellor (1975) and Narita (1980) have discussed the effects of tensile stresses in uniform snow, but we are not aware of any experiments investigating the tensile strength of weak snow layers. Our experiments indicate that higher vibration-induced tensile stress (~1 kPa) can be sufficient to fracture snow, even without shearing. Moreover, we should note that, in accordance with the empirical function for tensile strength as a function of snow density (Jamieson and Johnston, 1990), our stresses are close to the tensile strength of low-density snow (0.4 kPa and 100 kg m^{-3} respectively).

When comparing all fractures along the weak layer and the bottom, differences in the shear strength are apparent for weak-layer fractures (Fig. 11). Fractures along the weak layer that formed under tension are weaker than fractures formed under compression (Fig. 11a). In contrast, failures at the bottom of the snowpack do not show this relationship (Fig. 11b). The principal structural characteristics of the snow in the vicinity of the shear planes could determine such differences in performance. Bottom fractures occurred within a uniform stratum of the snow block or at the boundary with the metal plate, whereas weak-layer fractures were always propagated in snow through a potential failure plane with stress concentration. The concentration of tensile stress around a crack tip should favour crack propagation in an inherently weaker plane than in stressed uniform material.

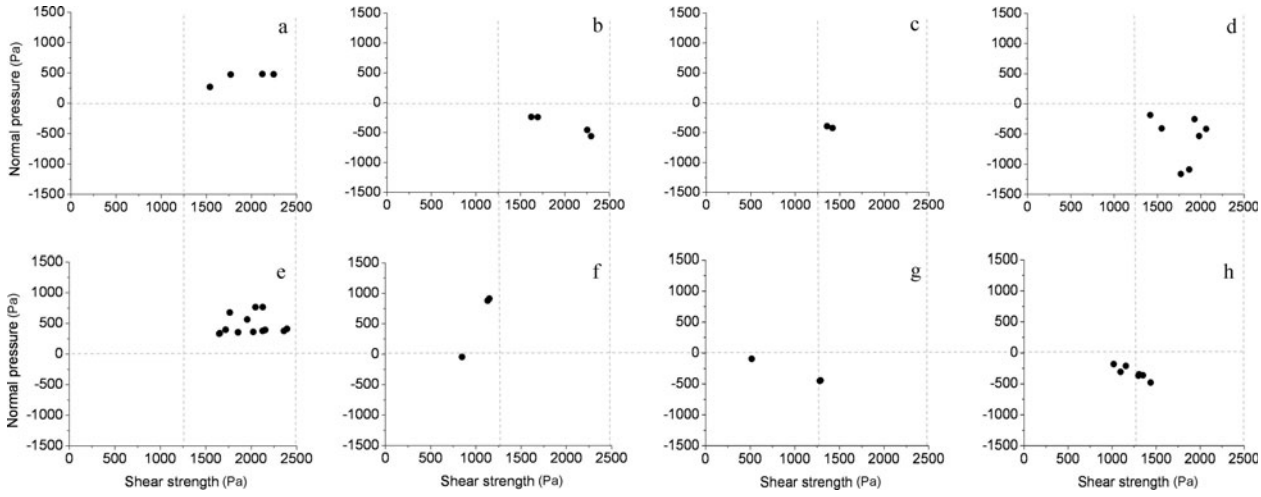

Fig. 10. Normal stress as a function of shear strength for different types of test (a positive normal stress represents compression; a negative stress represents tension). (a) Single degree-of-freedom bottom fracture, inclination 0°; (b) single degree-of-freedom bottom fracture, inclination 25°; (c) single degree-of-freedom bottom fracture, inclination 35°; (d) double degree-of-freedom bottom fracture, inclination 0°; (e) single degree-of-freedom weak-layer fracture, inclination 0°; (f) single degree-of-freedom weak-layer fracture, inclination 25°; (g) single degree-of-freedom weak-layer fracture, inclination 35°; (h) double degree-of-freedom weak-layer fracture, inclination 0°.

https://doi.org/10.3189/002214310792447833 Published online by Cambridge University Press

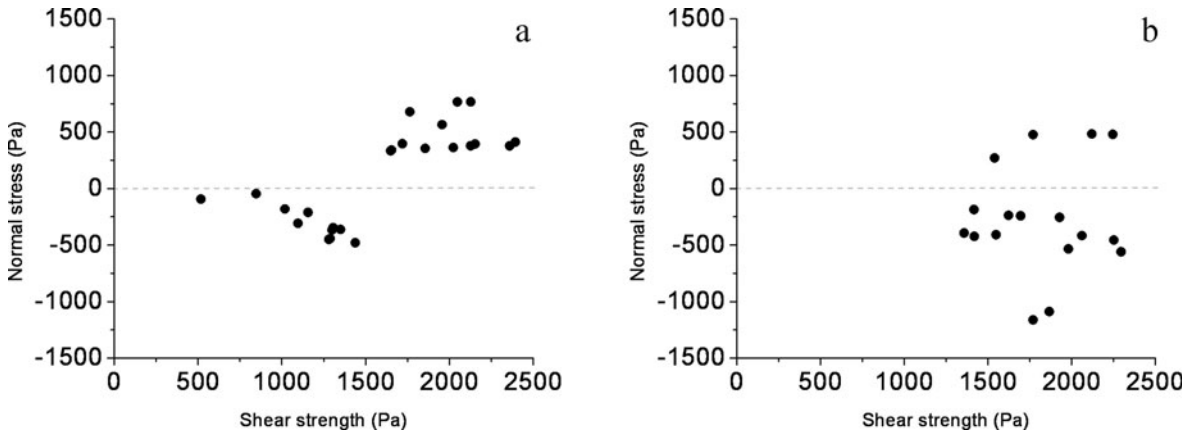

Fig. 11. Calculated shear strengths for (a) the weak layer and (b) the bottom compared with the normal stress at the moment of fracture for all tests (a positive normal stress represents compression; a negative stress represents tension).

We suggest that stratified snow is stronger in tests without tension and weaker in tests with a tensile component of stress. Indeed, for a brittle material such as snow, a high-rate tensional stress normal to the shear plane may be important and contribute to the nucleation of shear failure. Furthermore, this condition is almost unique to snow, being uncommon in rocks and other porous materials because their tensile strength is an order of magnitude larger than for snow (MPa compared with kPa) and because the earthquake-induced tensile stress reaches a critical level of snow strength. For example, because of the high strength of other engineering materials (e.g. rocks) and as a result of the significant underestimation of possible maximum values of the vertical component of acceleration, vertical accelerations were ignored until the 1960s and were not included in building codes (Newmark and Rosenblueth, 1971). Of relevance here is the recent extreme of 3.8 g vertical acceleration during the Iwate–Miyagi earthquake, as reported by Aoi and others (2008).

3.2.5. Shear strength and the duration of vibrating

One interesting observation was made with regard to the shear strength of snow and the duration of vibrating. If we consider the double degree-of-freedom tests, with fracturing along the weak layer, normal stress oscillations and a lengthy period of vibrations, we obtained a correlation coefficient of 0.84 (for seven samples) between the shear strength and duration of vibrating, indicating a possible linear relationship (Table 3).

The calculated shear strength becomes smaller with smaller periods of vibration (from 21.5 to 2.2 s), possibly related to the well-established effects of densification of soils, when for example sands, soils or clays consolidate, compact and settle when subjected to intense vibrations. Based on this assumption and the fact that snow crystals in the weak layers are full of voids between dendrites (Fig. 1), we suggest that ground vibrations (if insufficient for fracturing) can increase the stability and strength of low-density snow layers (as suggested by Podolskiy and others, 2010) by settling and increasing the density, thereby increasing the size and number of snow-grain bonds per unit volume. Therefore, two processes, controlled by the magnitude of earthquake and shaking duration, affect the properties of the snow, although they require further clarification and study. These processes probably help to stabilize a slope after seismicity that has not triggered an avalanche.

3.3. Simplified applications of the experimental data

It is interesting to apply the results of our experiments to a snowpack on an inclined slope subjected to realistic acceleration and using the simple inverse method (i.e. determine critical amount of snow, m_f, through known shear strength, τ, and some assumed peak acceleration, a_p; Equation (1)). If we assume typical values for horizontal accelerations during a strong earthquake (acting perpendicular to the slope), a surface slope angle of 38° (typical for most dry-slab avalanches; Perla, 1977) and snow with the same densities as those we measured in fractured blocks as well as the corresponding shear strength values for the snow, we can estimate a critical thickness for the snow covering the weak layer by

$$h_{cr} = \frac{m_f}{\rho A}, \tag{7}$$

where m_f can be extracted from Equation (3). This gives

$$m_f = \frac{\tau_{st} A}{g(\sin\alpha + a_p \cos\alpha)} \tag{8}$$

and Equation (7) now becomes

$$h_{cr} = \frac{\tau_{st}}{g\rho(\sin\alpha + a_p \cos\alpha)}, \tag{9}$$

where ρ is the density of the snow covering the weak layer, a_p is the peak horizontal acceleration (here we assume 0.5 g as the most commonly mapped value for strong earthquake hazard assessment (e.g. Giardini and others, 2003)), and α is the slope angle (assume 38°) (Table 3). For example, a peak horizontal acceleration of 0.5 g will create a critical situation for a weak layer with a shear strength of 1.2 kPa (average) given 0.58 m of snow cover (Fig. 12). Figure 13 shows the relationship between a wider range of horizontal accelerations (0–1 g) and slope inclinations (17–60°) for the same snow in each case. These examples demonstrate that typical realistic values (of acceleration and shear strength) can lead to unstable situations.

The same simplified approach can be used to estimate the accelerations that affected the slope at the moment of snow fracturing during the 1964 Great Alaskan Earthquake (at that time there were no seismic instruments capable of recording strong ground motion; Krauskopf, 1968). It is possible that

https://doi.org/10.3189/002214310792447833 Published online by Cambridge University Press

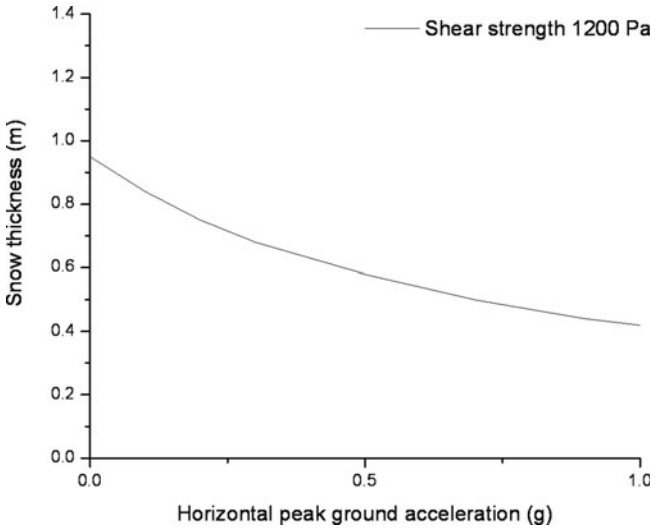

Fig. 12. Snow thickness as a function of horizontal peak ground acceleration (for shear strength 1200 Pa, shear plane inclined at 38°, density 210 kg m^{-3}). Curve shows the snow thickness required for failure, i.e. critical thickness values for fracture, over the range of horizontal peak accelerations.

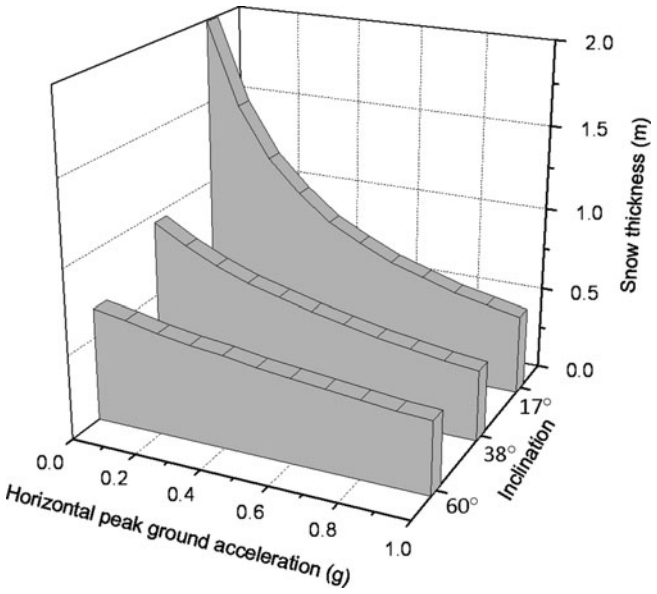

Fig. 13. Critical value of snow thickness (density 210 kg m^{-3}) for various accelerations (0–1 g) and slope inclinations (17°, 38° and 60°) over a weak layer with a shear strength of 1200 Pa.

the calculations could be based on an analysis of the photographs published by LaChapelle (1968), although there are too many unknown parameters to enable precise results to be attained.

4. SUMMARY

We have described experiments with snow on a shaking table in an attempt to understand the mechanisms involved in earthquake-induced avalanches. We employed various new approaches such as using specially prepared artificial snowpack 'sandwiches' that contained a weak layer and calculating the stresses produced by inertia for single degree-of-freedom vibrations with the shaking platform set at various angles, and for double degree-of-freedom oscillations. Our experimental results help confirm, demonstrate and support the following conclusions:

1. Shaking during strong ground motion can produce fracturing within a homogeneous or stratified snow block as a result of the inertial forces induced by acceleration.
2. In common with our shaking-table experiments, the stress tensor produced during the loading of snow, consequential to an earthquake, has shear, tensile and compressive components.
3. It is usually the case that avalanches associated with natural triggers or human activity occur with a positive normal stress (compression). In contrast, a high-rate tensional force oriented normal to the shear plane is possible only during earthquakes, not during other natural processes. This tension can be an important factor in the nucleation of certain fractures in the snow which are almost unique because brittle snow is one of the weakest materials under tension known in geology. Although such fracturing is uncommon in other materials, cohesive sand and piles of ash probably behave similarly.
4. The shear strength of a weak layer is smaller under tensile stress (more pure tensile tests and compression-shear tests are needed for construction of a dynamic Mohr-Coulomb failure envelope).
5. It is likely that prolonged vibrations (responsible for normal stress oscillations but insufficient for failure) can increase the shear strength of snow.
6. Shaking may contribute significantly to the initial stages of snow slab disintegration and accordingly may influence the avalanche flow parameters (it is likely that the coefficient of kinetic friction is affected, as rapid shattering of the original slab will provide smaller particles at the initial stages of motion).

Further work is needed for a better understanding of how strong ground motion influences the stability of snowpacks on a larger scale. We then need to investigate how to incorporate knowledge into avalanche forecasting. Ideally, the Kyoshin net (K-NET), which transmits strong-motion data on the Internet in real time, coupled with a snowpack model (e.g. SNOWPACK; Bartelt and Lehning, 2002) could provide useful information about the probability of collapse on a snow-covered slope before the arrival of S-waves. However, in the meantime, predictions of earthquake-induced avalanches remain a problem for the future.

ACKNOWLEDGEMENTS

We thank P. Bartelt and T.H. Jacka for editorial assistance. The initial version of this paper benefited enormously from extensive reviews by T. Faug and an anonymous reviewer. We thank S. Mochizuki and G. Okawa for support during experiments. We acknowledge technical support and provision of equipment from K. Shinbori, who engineered the shaking table, and from K. Kosugi, who assisted with high-speed video processing. These experiments would not have been possible without permission from T. Sato to use the CES facility. This work was supported by Grants-in-Aid for

https://doi.org/10.3189/002214310792447833 Published online by Cambridge University Press

Scientific Research (18651093), by a grant of the Russian Foundation for Basic Research (05-05-64368-A), and by a scholarship for foreign students provided by the Ministry of Education, Culture, Sports, Science and Technology, Japan. We also thank D.A. Short and A. Stallard for improvements to our written English.

REFERENCES

Abe, O. and T. Nakamura. 2005. Shear fracture strength of snow measured by the horizontal vibration method. *J. Snow Eng.*, **21**(4), 11–12. [In Japanese.]

Anderson, J.G. 2003. Strong-motion seismology. *In* Lee, W.H.K., H. Kanamori, P.C. Jennings and C. Kisslinger, *eds. International handbook of earthquake and engineering seismology, part B*. London, etc., Academic Press. (International Geophysics 81.)

Aoi, S., T. Kanugi and H. Fujiwara. 2008. Trampoline effect in extreme ground motion. *Science,* **322**(5902), 727–730.

Asano, S., S. Matsuura, T. Okamoto and K. Matsuyama. 2003. Shaking table tests to measure the underground displacement of the slope. *J. Jpn Landslide Soc.,* **40**(2), 134–137.

Bartelt, P. and M. Lehning. 2002. A physical SNOWPACK model for the Swiss avalanche warning. Part I: numerical model. *Cold Reg. Sci. Technol.,* **35**(3), 123–145.

Chernous, P., Y. Zuzin, E. Mokrov, G. Kalabin, Y. Fedorenko and E. Husebye. 1999. Avalanche hazards in Khibiny Massif, Kola, and the new Nansen Seismograph Station. *IRIS Newsl.,* **18**(1), 12–13.

Chernous, P., E. Mokrov, Y. Fedorenko, E. Husebye and E. Beketova. 2002. Russian–Norwegian project on seismicity-induced avalanches. *In* Stevens, J.R., *ed. Proceedings of the International Snow Science Workshop, 29 September–4 October 2002, Penticton, British Columbia*. Victoria, BC, British Columbia Ministry of Transportation Snow Avalanche Programs, 25–30.

Chernous, P.A., Yu.V. Fedorenko, E.G. Mokrov, N.V. Barashev, E. Hewsby and E.B. Beketova. 2004. Issledovanie vliyaniya seismichnosti na obrazovanie lavin [Study of seismicity effect on avalanche origin]. *Mater. Glyatsiol. Issled./Data Glaciol. Stud.* 96, 167–174. [In Russian with English summary.]

Chernous, P., Yu. Fedorenko, E. Mokrov and N. Barashev. 2006. Studies of seismic effects on snow stability on mountain slopes. *Polar Meteorol. Glaciol.,* **20**, 62–73.

Fierz, C. *and 8 others.* 2009. *The international classification for seasonal snow on the ground.* Paris, UNESCO–International Hydrological Programme (IHP Technical Documents in Hydrology 83.)

Föhn, P. and C. Camponovo. 1997. Improvements by measuring shear strength of weak layers. *In Proceedings of the International Snow Science Workshop, 6–11 October 1996, Banff, Alberta*. Revelstoke, B.C., Canadian Avalanche Association, 158–162.

Giardini, D., G. Gruenthal, K. Shedlock and P. Zhang. 2003. The GSHAP global seismic hazard map. *In* Lee, W.H.K., H. Kanamori, P.C. Jennings and C. Kisslinger, *eds. International handbook of earthquake and engineering seismology, Part B*. London, etc., Academic Press, 1233–1239.

Higashiura, M., T. Nakamura, H. Nakamura and O. Abe. 1979. An avalanche caused by an earthquake. *Rep. Nat. Res. Cent. Disaster Prev.* 21, 103–112. [In Japanese with English summary.]

Jamieson, J.B. and C.D. Johnston. 1990. In-situ tensile strength of snowpack layers. *J. Glaciol.*, **36**(122), 102–106.

Kinosita, S. and G. Wakahama. 1960. Thin sections of deposited snow made by the use of aniline. *Contrib. Inst. Low Temp. Sci., Ser. A 15, 35–45.*

Kramer, S.L. 1996. *Geotechnical earthquake engineering.* Englewood Cliffs, NJ, Prentice Hall.

Krauskopf, K.B. 1968. Preface. *In The Great Alaska Earthquake of 1964. Vol. 3: Hydrology, Part A.* Washington, DC, National Academy of Sciences. (NAS Publication 1603.)

LaChapelle, E.R. 1968. The character of snow avalanching induced by the Alaska earthquake. *In The Great Alaska Earthquake of 1964. Vol. 3: Hydrology, Part A.* Washington, DC, National Academy of Sciences, 355–361. (NAS Publication 1603.)

Matsuzawa, M., Y. Kajiya and Y. Ito. 2007. Assessment of snow safety factor under earthquake. *Snow Ice Hokkaido,* **26**, 95–98. [In Japanese.]

Mellor, M. 1975. A review of basic snow mechanics. *IAHS Publ.* 114 (Symposium at Grindelwald 1974 – *Snow Mechanics*), 251–291.

Mokrov, E.G. 2008. *Seismicheskie faktory lavinoobrazovaniya [Seismic factors of avalanche release]*. Moscow, Nauchniy Mir. [In Russian with English summary.]

Nakamura, T., O. Abe, R. Hashimoto and T. Ohta. 2010. A dynamic method to measure the shear strength of snow. *J. Glaciol.*, **56**(196), 333–338.

Narita, H. 1980. Mechanical behaviour and structure of snow under uniaxial tensile stress. *J. Glaciol.,* **26**(94), 275–282.

Newmark, N.M. and E. Rosenblueth. 1971. *Fundamentals of earthquake engineering.* Englewood Cliffs, NJ, Prentice-Hall.

Ogura, Y., K. Izumi, N. Miyazaki and S. Kobayashi. 2001. An avalanche caused by an earthquake at Nakazato village, Niigata Prefecture, on January 4th 2001. *Annu. Rep. Res. Inst. Hazards Snowy Areas, Niigata Univ.*, **23**, 9–15. [In Japanese with English summary.]

Perla, R. 1977. Slab avalanche measurements. *Can. Geotech. J.,* **14**(2), 206–213.

Podolskiy, E.A., K. Nishimura, O. Abe and P.A. Chernous. 2010. Earthquake-induced snow avalanches: I. Historical case studies. *J. Glaciol.,* **56**(197), 431–446.

Reitherman, R. 1997. *The 1998 CUREe Calendar: historic developments in the evolution of earthquake engineering.* Richmond, CA, Consortium of Universities for Research in Earthquake Engineering.

Schweizer, J., J.B. Jamieson and M. Schneebeli. 2003. Snow avalanche formation. *Rev. Geophys.,* **41**(4), 1016. (10.1029/2002RG000123.)

Singh, A. and A. Ganju. 2002. Earthquakes and avalanches in western Himalaya. *In* Paul, D.K., A. Kumar and M.L. Sharma, *eds. Proceedings of the 12th Symposium on Earthquake Engineering, 16–18 December, 2002, Roorkee, India*. Roorkee, Indian Institute of Technology.

Tarr, R.S. and L. Martin. 1914. Alaskan glacier studies of the National Geographic Society in the Yakutat Bay, Prince William Sound and Lower Copper River regions. Washington, DC, National Geographic Society.

Voitkovsky, K.F., A.N. Bozhinsky, V.N. Golubev, M.N. Laptev, A.A. Zhigulsky and Y. Slesarenko. 1975. Creep-induced changes in structure and density of snow. *IAHS Publ.* 114 (Symposium at Grindelwald 1974 – *Snow Mechanics*), 171–179.

MS received 2 November 2009 and accepted in revised form 10 May 2010